Evaluation of Fracture Toughness of Porous Ceramics*

Yoshihisa SAKAIDA** and Keisuke TANAKA***

The indentation fracture (IF) method, the single-edge precracked beam (SEPB) method, and the single-edge V-notched beam (SEVNB) method were applied to evaluate the fracture toughness of four kinds of porous ceramics of SiC, Al_2O_3 and $Mg_2Al_4Si_5O_{18}$ with porosity ranging from 37 to 43%. The microstructures of these materials were composed of ceramics grains, glassy grain boundaries and pores. Each grain was joined together with the glassy grain boundary phase. The IF and SEPB methods were not applicable because both precracks and indenter traces were not visible. On the other hand, the SEVNB method was applicable because the V-notch could be easily machined by grinding. In the case of the SEVNB method, the applied load versus back-face strain plots under four-point bending showed nonlinearity prior to the maximum load. The R-curve behavior was estimated from the compliance change of specimens. The fracture toughness of porous ceramics was smaller than that of dense ceramics, and increased with increasing crack extension. Since the stable crack predominantly propagated along glassy grain boundaries, the R-curve behavior depended on the loading rate and matrix grain size. The increment of the R-curve by grain bridging became larger for coarser-grain sized ceramics.

Key Words: Porous Ceramics, Fracture Toughness, Indentation Fracture Method, Single-edge Precrack Beam Method, Single-edge V-notched Beam Method, R-curve Behavior

1. Introduction

Recently, porous ceramics of about 40% porosity are noticed as dedusting filters for high-temperature turbines[1],[2]. However, there are few research studies on the mechanical properties and fracture behavior of porous ceramics[3],[4]. Therefore, in the present study, the conventional testing methods for fracture toughness of dense ceramics such as the IF method (Indentation Fracture method), the SEPB method (Single-Edge Precracked Beam method) and the SEVNB method (Single-Edge V-notched Beam method[5]) were first examined for application to typical porous ceramics with porosity ranging from 37 to 43%. Next, the R-curve behavior of porous ceramics was measured by the compliance method using back-face strains of the SEVNB specimen[3], and then the effect of the microstructure of porous ceramics on fracture toughness and behavior was examined.

2. Experimental Procedure

2.1 Materials

The materials used in the present study were the sum total of four types of porous ceramics of one silicon carbide (KD-DSL T10-20, manufactured by Schumacher U & T in Germany[4]), two kinds of alumina (FA10 and FA4, manufactured by Kyocera Co. in Japan) and one cordierite (manufactured by Kyocera Co. in Japan). They are simply designated as SiC, Al_2O_3(A), Al_2O_3(B) and $Mg_2Al_4Si_5O_{18}$. The mean pore size, porosity, density and bending strength of each material are summarized in Table 1. Figure 1 shows the SEM microstructures of porous ceramics. The porosity of each material is around 40%, while the microstructures are significant different depending

* Received 12th September, 2002 (No. 00-1522). Japanese original: Trans. Jpn. Soc. Mech. Eng., Vol. 67, No. 660, A (2001), pp. 1378-1385 (Received 14th December, 2000)

** Department of Mechanical Engineering, Faculty of Engineering, Shizuoka University, 3-5-1 Johoku, Hamamatsu 432-8561, Japan. E-mail: tysakai@ipc.shizuoka.ac.jp

*** Department of Mechanical Engineering, Faculty of Engineering, Nagoya University, Furou-cho, Chikusa-ku, Nagoya 464-8603, Japan

Table 1 Properties of porous ceramics

	Mean pore size (μm)	Porosity (%)	Density (g/cm³)	Bending strength (MPa)
SiC	41	37	1.96	11.1
Al_2O_3(A)	1.3	43	2.26	30.3
Al_2O_3(B)	18	38	2.39	30.0
$Mg_2Al_4Si_5O_{18}$	25	43	1.61	13.0

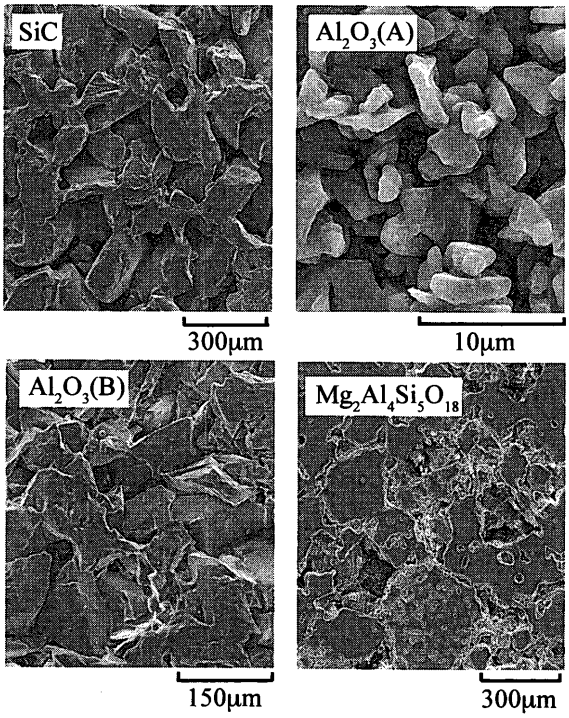

Fig. 1 Microstructures of porous ceramics

on the morphology of the matrix ceramic grains. Figure 2 shows the grain diameter distribution on the assumption that the shape of the matrix ceramic grain is spherical. The microstructures of these materials were composed of ceramics grains, glassy grain boundaries and pores. The grains of the SiC sample are of silicon carbide whose mean size is about 192 μm. The grains of Al_2O_3(A) and Al_2O_3(B) samples are of alumina whose mean sizes are about 4.7 and 72 μm, respectively. On the other hand, the grains of the $Mg_2Al_4Si_5O_{18}$ sample are of the mixture of minute primary grains of about 1 μm and secondary grains of about 143 μm, and the size of the pores between primary grains is about 3 μm. The pore with a diameter of about 25 μm, as shown in Table 1, corresponds to that between secondary grains. Each grain of these materials is joined together with a glassy grain boundary phase[4], and its bonding-strength is very weak.

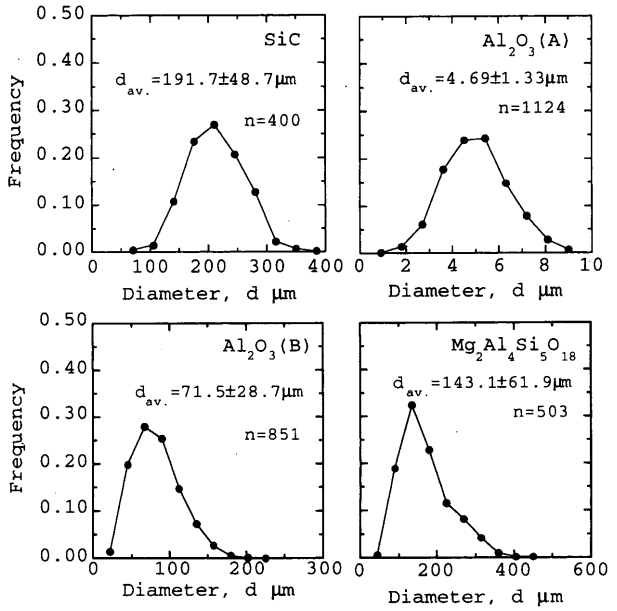

Fig. 2 Distribution in grain diameter of porous ceramics

2.2 Specimens and measurement of fracture toughness and *R*-curve behavior

The IF, SEPB and SEVNB methods were first applied to porous ceramics for evaluating fracture toughness. In the case of the IF and SEPB methods, the bend-bar specimens with a width of 3 mm, a thickness of 4 mm, and a length of 40 mm were used in conformity with JIS R 1607. For the IF method, the testing surface of the bend-bar specimen was mechanically polished with diamond slurry to be as fine as possible, and then was indented using a Vickers indenter. For the SEPB method, three Vickers indentations were introduced at the center of the specimen at a normal load, $P=98$ N, as a starter of the precrack, and then the pop-in precrack was introduced by the bridge-indentation (BI) method using an acoustic emission (AE) sensor cemented on the precracker.

In the case of the SEVNB method, the single-edge V-notched beam specimens with a width of 5 mm, a thickness of 7 mm, and a length of 45 mm were used. V-notches were machined by grinding using a V-shaped diamond wheel[5], as shown in Fig. 3. The range of V-notch depths was from 0.67 to 4.93 mm. The radius of the notch root curvature was about 20 μm. The SEVNB method was carried out in either air or water at room temperature under four-point bending, as shown in Fig. 4. The inner and outer spans were 20 and 40 mm, respectively. During loading, the bending load and the back-face strain were monitored using a strain gauge cemented on the SEVNB specimens. The crosshead speed, *CHS*, ranged from 0.005 to 0.5 mm/min.

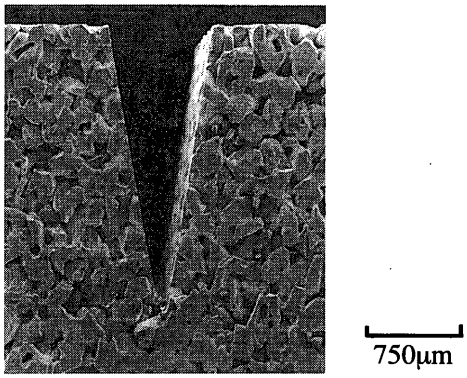

Fig. 3 V-notch in the SEVNB specimen of porous SiC

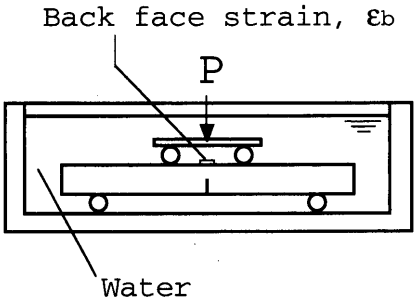

Fig. 4 Schema of the SEVNB method in water

3. Experimental Results and Discussion

3.1 IF method

Using SiC and Al_2O_3(A) samples in which mean pore sizes were maximum and minimum in four types of porous ceramics, the IF method was carried out for evaluating fracture toughness.

To begin with, a Vickers indenter was impressed on the surface of the SiC specimen at P=9.8 and 4.9 N. As the result, near the impressed area, almost all the pores were squashed and SiC particles sank significantly, so that both the indentation trace and Vickers-induced surface cracks were not visible. Then, the Vickers indenter was directly impressed on a SiC particle with a small indentation load to measure the fracture toughness of the matrix SiC grain. Figure 5 shows the SEM micrograph of the indentation in SiC particle at P=2.9 N. In order to evaluate the fracture toughness of the matrix ceramic grain, the radial/median crack lengths that arose from the four corners of the indentation trace must be measured. Using a scanning electron microscope, only the indentation trace could be identified, while the Vickers-induced surface cracks could not be discriminated. Furthermore, the subsurface particle shape was obscure so that the flaw shape could not be specified. Therefore, the fracture toughness of the matrix grain in porous ceramics could not always be evaluated, even if the Vickers-induced surface cracks could be

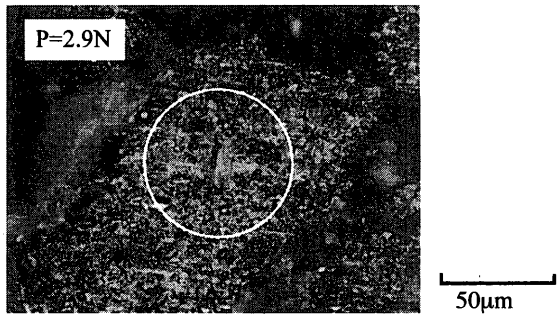

Fig. 5 Micrograph of Vickers indent in porous SiC

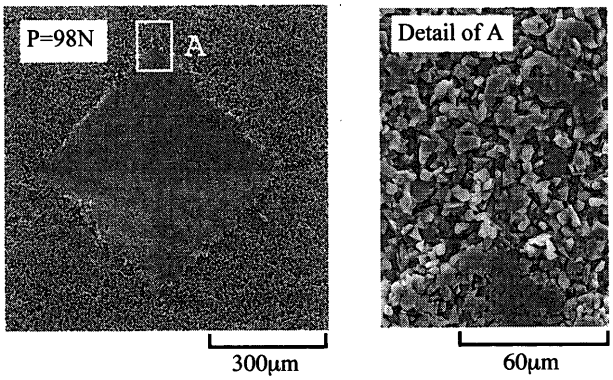

Fig. 6 Micrograph of Vickers indent in porous Al_2O_3(A)

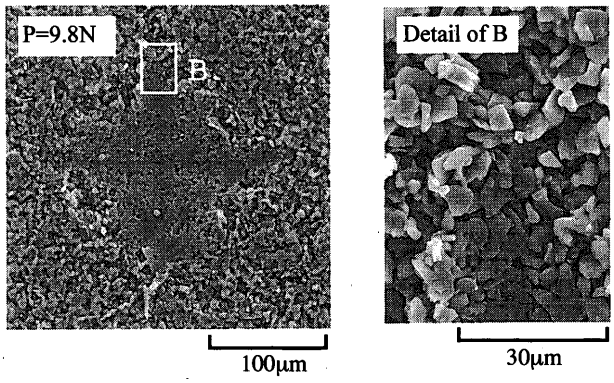

Fig. 7 Micrograph of Vickers indent in porous Al_2O_3(A)

observed.

Next, the Vickers indenter was impressed on the surface of the Al_2O_3(A) specimen at P=98 and 9.8 N. Figure 6 shows the SEM micrographs around the indentation at P=98 N. The indentation trace was more distinct in comparison with that of the SiC sample. However, Vickers-induced surface cracks were not visible (see the detailed photograph of A in Fig. 6). Figure 7 shows the SEM micrographs around the indentation at P=9.8 N. Under the condition of decreasing the indentation load, the indentation crack was still invisible.

It was concluded that the fracture toughness testing using the IF technique was inapplicable to

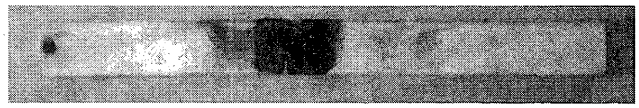

Fig. 8 Appearance of the SEPB specimen stained with red ink

evaluate the fracture toughness for porous ceramics.

3.2 SEPB method

In the case of the SEPB method, using either a machined straight-through notch or indentation cracks as a starter of the precrack, the pop-in precracks are usually introduced by the bridge-indentation (BI) method. Therefore, both introduction and identification of the pop-in precrack are key technologies for evaluating the fracture toughness using the SEPB technique.

Whether the pop-in precrack was introduced in the SiC specimen with the maximum mean pore size was first examined. After the precracking procedure, oily ink soaked into the entire specimen to say nothing of precrack by capillarity, because pores of about 41 μm was enough size to permeate oily ink into the entire material. Therefore, it is impossible to dye the precrack alone in the SiC specimen.

Next, the precrack introduction testing using the BI technique was carried out for the Al_2O_3(A) specimen with the minimum pore size. The pop-in signal could not be detected regardless of the testing load, because the event level of AE was very low during testing. The pop-in crack could not be observed at all from the testpiece side. In the present study, after compressive loading to a constant load level on the precracker, oily ink was made to soak from the testpiece side. Figure 8 shows one example of stained SEPB specimens with red ink. The red ink permeated into the entire specimen as well as into the SiC sample, although the mean pore size of the Al_2O_3(A) specimen was very small of 1.3 μm. The existence and crack length of precrack could not be measured.

It was concluded that the fracture toughness testing using the SEPB technique was also inapplicable to evaluate the fracture toughness for porous ceramics.

3.3 SEVNB method

In the case of the SEVNB method, it is possible to use the notch as a precrack, if the V-notch can be machined as shown in Fig. 3. Furthermore, the notch depth can be easily measured using a profile projector. Therefore, the SEVNB method would be applicable to evaluate the fracture toughness for porous ceramics having high porosity and low fracture strength such as the present materials.

Figures 9 and 10 show typical applied load versus displacement and applied load versus back-face strain

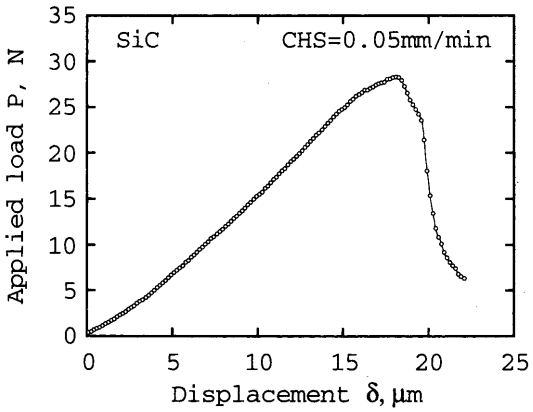

Fig. 9 Applied load vs. displacement curve for SiC

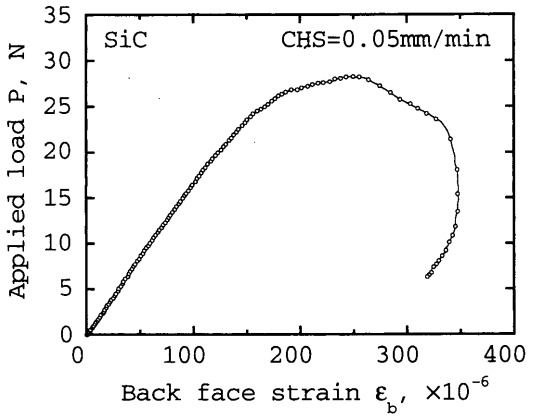

Fig. 10 Applied load vs. back-face strain curve for SiC

plots during loading for the SiC sample. Both relationships showed nonlinearity before reaching the maximum load. The SEVNB specimens were not broken unstably after reaching the maximum load. According to the *in-situ* observation of the same material reported by Song and Takeda[6], microcracks were generated from the V-notch tip before reaching the maximum load, and propagated stably. Consequently, the applied load versus back-face strain plots seem to become nonlinear. Furthermore, the broken pieces of the SEVNB specimen were still undivided after unloading, even if the main crack propagated to the compression side. The fracture surfaces clung to each other. Figure 11(a) shows the SEM micrograph of the side-view of broken pieces after the fracture toughness test. The main crack that arose from the notch tip propagated along the interface between matrix SiC grains, and was bridged by some grains across the crack faces. Figure 11(b) shows the fracture surface near the V-notch tip that was divided compulsorily. In this figure, there were few grains fractured transgranularly. It was found that fracture surface of porous ceramics was formed as a result of selective fracture of the glassy grain bound-

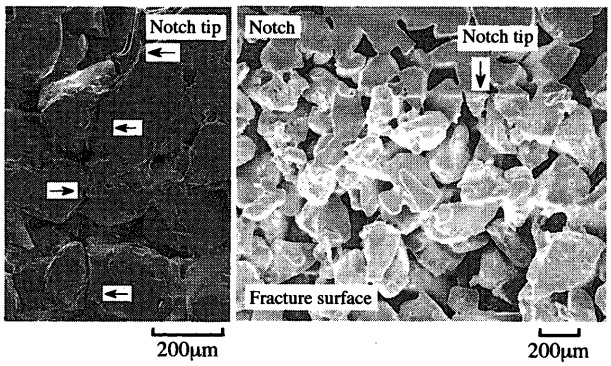

(a) Crack path (b) Fracture surface near the notch tip

Fig. 11 Fracture surface of porous SiC

aries that joined SiC grains.

For dense ceramics in which the microcrack stably propagated from the notch tip, the fracture toughness characteristic could be directly evaluated as R-curve behavior from the side-view observation of the crack tip using an optical microscope[7],[8]. However, in the case of porous ceramics, it is difficult to directly observe the crack tip from the side-view of the specimen because of high porosity. In the present study, crack extension was estimated by the compliance method using back-face strain, and then R-curve behavior was evaluated. The details are described in the appendix.

3.4 R-curve behavior of each material

3.4.1 R-curve behavior of SiC sample Figure 12 shows R-curves, K_R, of SiC specimens at $a_0/W=0.41$ together with the applied stress intensity factor, K_{app}-curve, at the maximum load. In this figure, the R-curves were estimated from the results on the condition that $CHS=0.5$ mm/min in air at room temperature, where a_0 is initial notch depth and W is thickness of the SEVNB specimen. R-curves overlapped one another. The average stress intensity factor, K_R, at the point where the K_{app}-curve at the maximum load came in contact with the K_R-curve was 0.55 MPa $\sqrt{\text{m}}$. This value was much smaller than the fracture toughness of a dense silicon carbide. The K_R-Δa relationship shows rising R-curve behavior, where Δa is a crack extension from the notch tip. The average amount of crack extension was 0.69 mm until the applied load reached a maximum. Figure 13 shows the R-curve behavior under several crosshead speeds. The initial stress intensity factor K_R at $\Delta a=0$ and the amount of crack extension at the maximum load, P_{max}, were nearly constant regardless of the crosshead speed. While, the increment of K_R for Δa on the slowest condition of $CHS=0.005$ mm/min was lower than that of others. The dependence of cross-

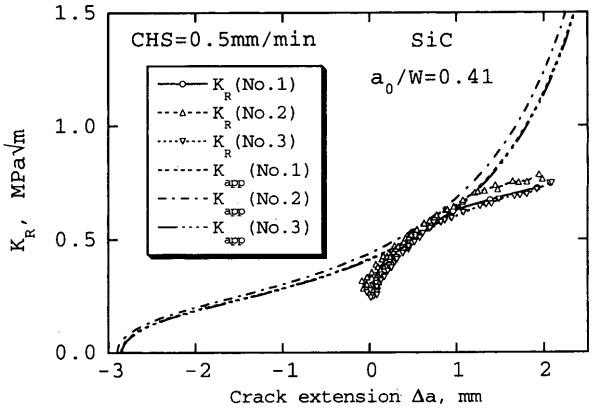

Fig. 12 R-curve behavior for porous SiC

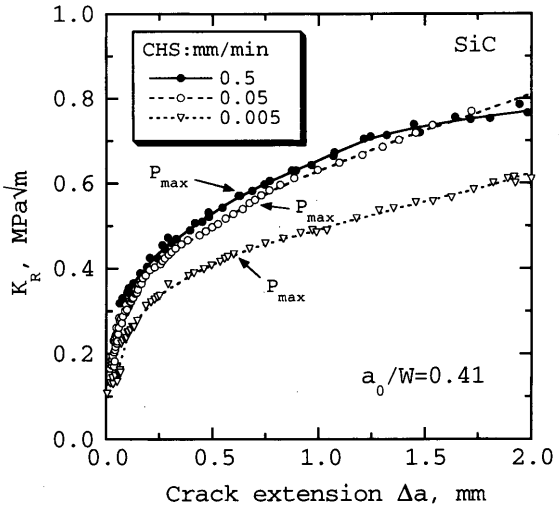

Fig. 13 R-curve behavior for porous SiC under several crosshead speeds

head speed on R-curve behavior has a close relation to a phenomenon of stress-corrosion-cracking, SCC, of glassy phase because fracture behavior of porous silicon carbide was controlled by the microfracture of glassy grain boundaries between SiC grains, as mentioned above in section 3.3.

Then, the fracture toughness test was carried out in water under the slowest crosshead speed of 0.005 mm/min, and then R-curve behavior in water was compared with that in air as shown in Fig. 14. The R-curve behavior in water overlapped with the result in air under the same crosshead speed. Figure 15 shows the relationship between CHS and K_R at $P=P_{max}$. From $CHS=0.05$ mm/min, the K_R value was nearly constant. On the other hand, at $CHS=0.005$ mm/min, the crack propagation rate was accelerated due to the SCC effect, and then the increment of K_R became smaller. The surface of the glassy phase between SiC grains had already adsorbed water since grain boundaries of the SiC sample were always exposed to air through the pores. Consequently, the R-curve in

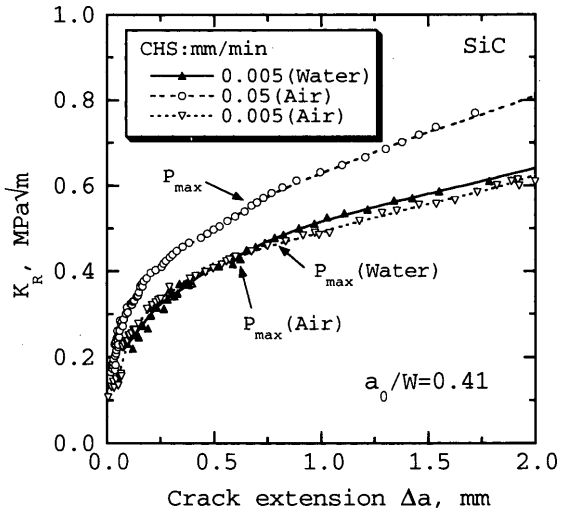

Fig. 14 R-curve behavior for porous SiC in water

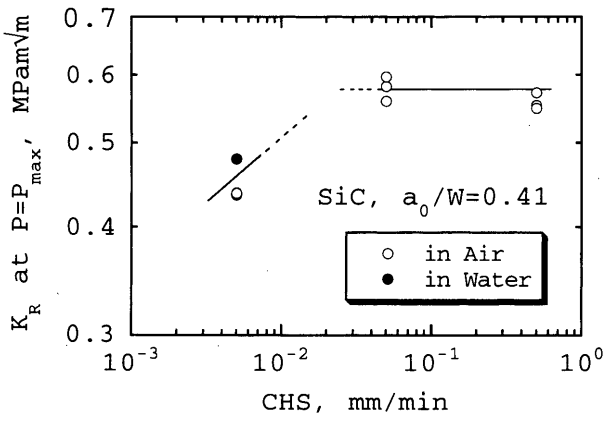

Fig. 15 Relationship between K_R and crosshead speed

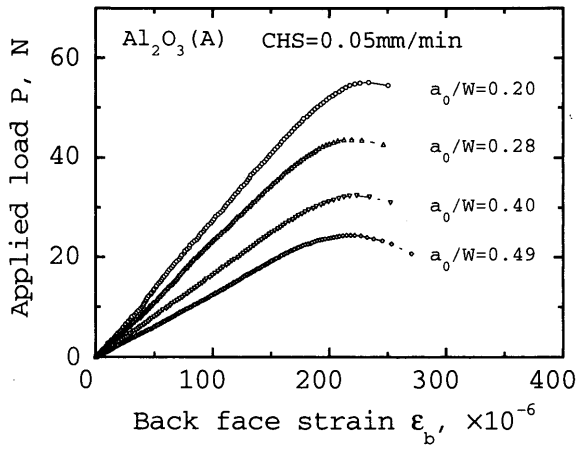

Fig. 16 Applied load vs. back-face strain curve of Al_2O_3(A)

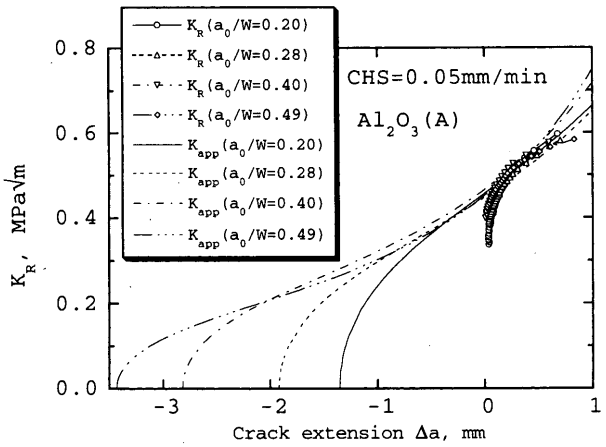

Fig. 17 R-curve behavior for porous Al_2O_3(A)

water seemed to overlap with that in air. Therefore, the loading condition of fracture toughness test for porous ceramics should be carefully determined because the *SCC* effect directly influences R-curve behavior. In the present study, the following fracture toughness tests were all carried out in air under $CHS=0.05$ mm/min.

3. 4. 2 R-curve of Al_2O_3(A) sample Figure 16 shows the relationship between the applied load and back-face strain of the Al_2O_3(A) sample, in which both pore and grain sizes were the smallest. In this figure, the result of the specimen with a different notch depth, a_0, is summarized. These curves, as well as those for the SiC sample, showed nonlinearity before reaching the maximum load. However, the change of the compliance of each specimen was slight, and it tended to unstably fracture immediately after reaching the maximum load.

Figure 17 shows R-curves, K_R, and K_{app}-curves at the maximum load. R-curves were estimated from the applied load versus back-face strain plots of Fig. 16. Although the compliance, λ, and its change differ by the notch depth, R-curves almost agreed with one another. The average K_R value, at which the K_{app}-curve met with the R-curve, was 0.52 MPa $\sqrt{\text{m}}$, and was also much smaller than the fracture toughness of dense alumina. The K_R-Δa relation showed rising R-curve behavior in the same manner as the SiC sample. In this case, the amount of crack extension until the maximum load was about from 0.24 to 0.45 mm, and then the average value was 0.32 mm.

Figure 18 shows the SEM micrographs of the side-view and fracture surface in the vicinity of the notch tip after the test. From a macroscopic point of view, the main crack that arose from the notch tip propagated straightly. The main crack microscopically propagated along the interface between matrix Al_2O_3 grains, and the fracture surface near the notch tip was entirely composed of intergranular facture surfaces. It was found that the fracture surface was formed as a result of the fracture of the glassy phase that connected Al_2O_3 grains. In this material, the

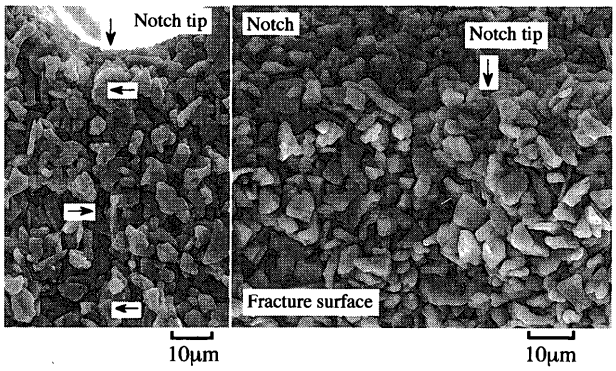

(a) Crack path (b) Fracture surface near the notch tip

Fig. 18 Fracture surface of porous Al_2O_3(A)

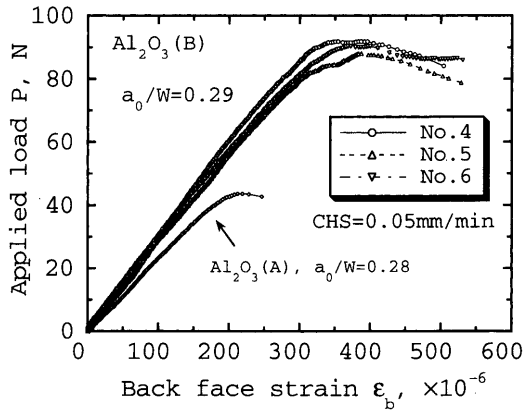

Fig. 19 Applied load vs. back-face strain curve of Al_2O_3(B)

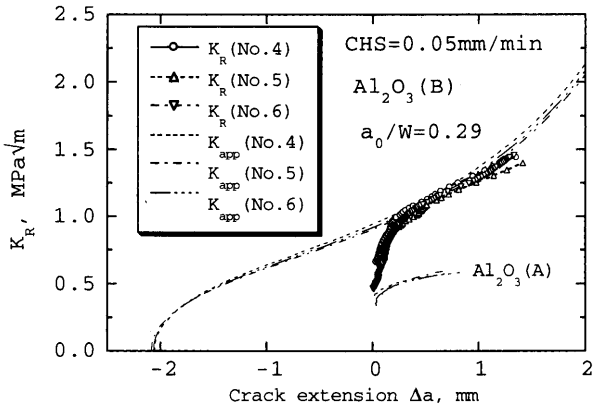

Fig. 20 R-curve behavior for porous Al_2O_3(B)

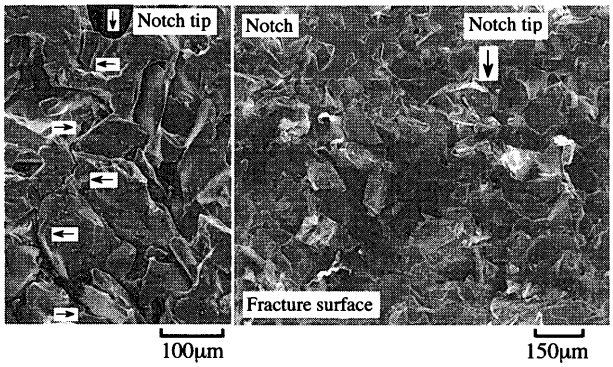

(a) Crack path (b) Fracture surface near the notch tip

Fig. 21 Fracture surface of porous Al_2O_3(B)

stress shielding effect of the crack tip due to grain bridging was relatively small because the matrix Al_2O_3 particle was very small with the mean grain size of 4.7 μm.

3.4.3 R-curve of Al_2O_3(B) sample Figure 19 shows the applied load versus back-face strain plots of the Al_2O_3(B) sample in comparison with the typical result of the Al_2O_3(A) sample. These curves for the Al_2O_3(B) sample showed nonlinearity before reaching the maximum load. Specimens were not broken unstably immediately after reaching the maximum load. The mean grain size of the Al_2O_3(B) sample was 72 μm, and was about 15 times larger than that of the Al_2O_3(A) sample. Furthermore, the maximum load was about 1.8 times higher than that of the Al_2O_3(A) sample although the initial compliance without crack growth, λ, was about 0.8 times higher. This is because of its slightly lower porosity of about 38% (see Table 1).

Figure 20 shows R-curves, K_R, and K_{app}-curves at the maximum load. R-curves were also estimated from the applied load versus back-face strain curves in Fig. 19, and were compared to the R-curve for the Al_2O_3(A) sample. R-curves overlapped one another, and the K_R-Δa relations showed rising R-curve behavior. The initial stress intensity factor K_R at $\Delta a=0$ coincided with that of the Al_2O_3(A) sample. While the average value of K_R at which the K_{app}-curve met with the R-curve was 1.15 MPa $\sqrt{\text{m}}$, and the average amount of crack extension before reaching the maximum load was about 0.59 mm. From the above experimental results, it was found that increment of K_R for Δa was larger than that of the Al_2O_3(A) sample.

Figure 21 shows the SEM micrographs of the side-view and fracture surface in the vicinity of the notch tip after the test. The main crack that arose from the notch tip propagated along grain boundaries between Al_2O_3 grains, and was bridged by some grains across the crack faces similar to the fracture of the SiC sample. It was found that this grain-bridging contributed to the rising of the R-curve. The fracture surface was also formed from intergranular fracture, though the morphologies of the matrix grain and pore of the Al_2O_3(B) sample were significantly different from the Al_2O_3(A) sample.

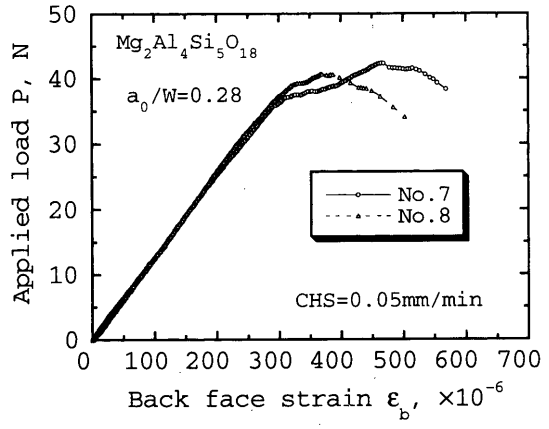

Fig. 22 Applied load vs. back-face strain curve of $Mg_2Al_4Si_5O_{18}$

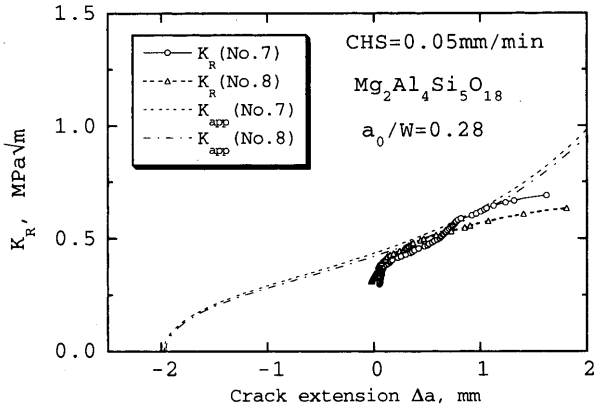

Fig. 23 R-curve behavior for porous $Mg_2Al_4Si_5O_{18}$

3.4.4 R-curve of $Mg_2Al_4Si_5O_{18}$ sample Figure 22 shows the applied load versus back-face strain plots of the $Mg_2Al_4Si_5O_{18}$ sample. The mean grain and pore sizes of secondary grains in the $Mg_2Al_4Si_5O_{18}$ sample were 143 and 25 μm, respectively. The secondary grain of the $Mg_2Al_4Si_5O_{18}$ sample was the second largest in the sample materials. Therefore, the load vs. back-face strain plots showed nonlinearity before reaching the maximum load, and specimens were not broken unstably immediately after reaching the maximum load as well as the case of the SiC sample.

Figure 23 shows R-curves and K_{app}-curves at the maximum load. R-curves of this material were also estimated from the applied load versus back-face strain curves in Fig. 22. The K_R-Δa relation showed rising R-curve behavior such as shown by other porous materials. The average value of K_R at which the K_{app}-curve met with the R-curve was 0.56 MPa $\sqrt{m}$, and the average amount of crack extension before reaching the maximum load was about 0.55 mm.

Figure 24 shows the SEM micrographs of the

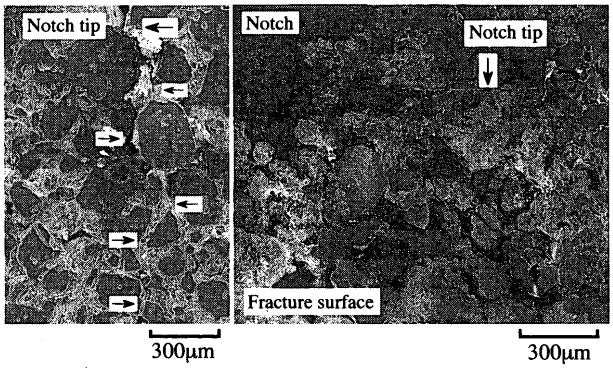

(a) Crack path (b) Fracture surface near the notch tip

Fig. 24 Fracture surface of porous $Mg_2Al_4Si_5O_{18}$

side-view and fracture surface in the vicinity of the notch tip after the test. The main crack that arose from the notch tip propagated along grain boundaries between the secondary grains in the $Mg_2Al_4Si_5O_{18}$ sample, and was bridged by some grains. It was found that the grain-bridging of secondary grains contributed to the rising of the R-curve. As mentioned above in section 2.1, the main pore that controls the permeability of the ceramic filter was made up of spaces between secondary grains, and the bonding strength of its grain boundary phase was very weak. Therefore, the main crack predominantly propagated along the grain boundaries between secondary grains. Transgranular fracture of secondary grains was observed in a few areas since the fracture strength of secondary grains was also weak.

From the above experimental results, it was concluded that R-curve behavior of porous ceramics could be evaluated by the compliance method using the applied load vs. back-face strain plot obtained from the fracture toughness test using the SEVNB technique.

3.5 Effect of microstructure on R-curve behavior

Figure 25 shows the relationship between mean grain size, d, and amount of crack extension, Δa, until the applied load reached the maximum for all samples. The Δa of the Al_2O_3(A) sample in which the matrix grain size is the smallest among the four types of porous ceramics was very short from 0.24 to 0.45 mm, and specimens were broken brittlely in a short time after reaching the maximum load. On the other hand, the Δa of the remaining three samples were slightly long from 0.55 to 0.69 mm. The main crack tended to propagate stably after reaching the maximum load, and specimens were difficult to break unstably. The fracture of porous ceramics propagated as a result of selective microfracture of the glassy

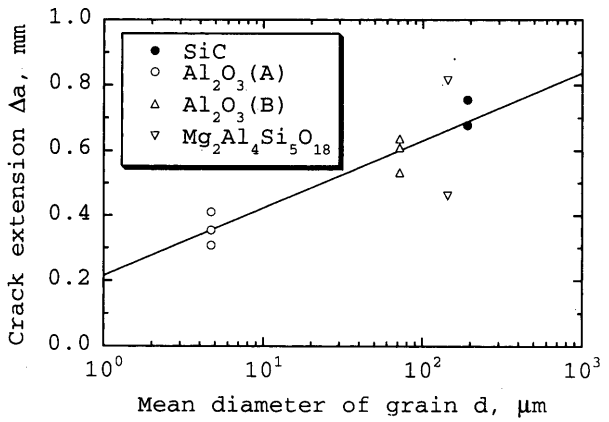

Fig. 25 Relationship between crack extension Δa and grain diameter d for porous ceramics

grain boundaries with a weakest bonding-strength. However, in the case of porous ceramics having very small matrix grains such as the Al_2O_3(A) sample, the main crack propagated straightly, and then did not contribute significantly to the rise in the R-curve. On the other hand, in the case of porous ceramics having very large matrix grains such as SiC, Al_2O_3(B) and $Mg_2Al_4Si_5O_{18}$ samples, the main crack made a detour around matrix grains, and was grain-bridged across the propagated crack faces. As a result, the R-curve rose with an increase in crack extension. It can be concluded that at the initiation of fracture in porous ceramics, the stable crack easily grows by the fracture of glassy grain boundaries since the bonding strength between matrix grains is very weak. R-curve behavior after crack growth is greatly dependent on the matrix grain size. It is found that the increment of the R-curve by grain bridging becomes larger for coarser-grain sized porous ceramics.

In the present study, the R-curve was estimated on the assumption that only one crack propagated straightly from the initial notch tip and crack extension was determined from the compliance change using back-face strain. Therefore, the amount of crack extension, Δa, might be slightly different from actual crack extension, when the crack detoured around large matrix grains. The effects of crack deflection and grain-bridging on either the compliance or R-curve behavior will be examined in the future.

4. Conclusions

The fracture toughness methods for porous ceramics were examined, and R-curve behavior of four kinds of porous ceramics was evaluated using the SEVNB technique. The results are summarized as follows:

(1) The IF and SEPB methods were inapplicable because it was difficult to introduce both indentation crack and pop-in crack in porous ceramics.

(2) The SEVNB method was applicable because the V-notch could be easily machined by grinding. R-curve behavior could be evaluated from the compliance change using the applied load versus back-face strain plot.

(3) Although the K_R value of porous ceramics at the maximum load was much smaller than the fracture toughness of dense ceramics, the K_R-Δa relationship showed rising R-curve behavior.

(4) The fracture of porous ceramics was controlled by the microfracture of glassy grain boundaries between matrix grains, so that the fracture propagated at the lower K_R value, the loading rate of fracture toughness test was slower.

(5) R-curve behavior after crack growth was greatly dependent on the matrix grain size. The increment of the R-curve by grain bridging was found to become larger for coarser-grain sized porous ceramics.

Acknowledgments

This research supported by NEDO, as a part of the Synergy Ceramics Project promoted by METI, Japan, is greatly appreciated.

Appendix: Evaluation of R-curve Behavior by Compliance Method Using Back-Face Strain

The compliance, λ, of the SEVNB specimen is expressed as

$$\lambda=\varepsilon_b/P \qquad (1)$$

where ε_b is back-face strain and P is bending load. The amount of crack extension, Δa, can be estimated from the above compliance change, if the relation of compliance, λ, for arbitrary crack length, a, can be obtained. In this study, the following equation that was derived by Tanaka et al.[3] from the finite element analysis was used

$$\lambda/\lambda_0=1.000\,7+0.045\,96\alpha+3.414\,8\alpha^2+94.986\alpha^3 -816.22\alpha^4+3\,433.3\alpha^5-8\,003\alpha^6+10\,740\alpha^7 -7\,801.4\alpha^8+2\,451.2\alpha^9 \qquad (2)$$

where λ_0 is compliance without notch, α $(=a/W)$ is dimensionless crack length, a is crack length and W is thickness of the SEVNB specimen. The λ_0 is given by

$$\lambda_0=\frac{3(S_1-S_2)}{2EBW^2} \qquad (3)$$

where E is Young's modulus, B is width of specimen, S_1 and S_2 are outer and inner spans, respectively.

Figure 26 shows the relationship between λ/λ_0 and α, as defined by Eq.(2). In this figure, the experimental data calculated from the applied load vs. back-face strain curve of each sample were plotted together. The experimental data agree very well with

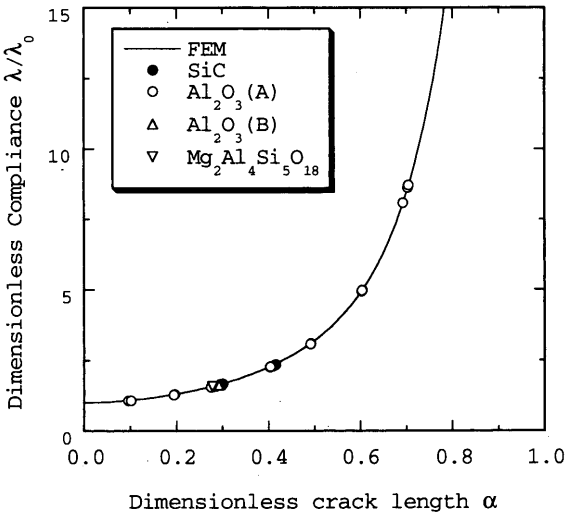

Fig. 26 Relationship between compliances and crack lengths for porous ceramics

the results of the finite element analysis. It was found that the amount of crack extension could be estimated from the change of back-face strain.

In the experiment, the initial compliance, λ, was first calculated from the slope of the applied load vs. back-face strain curve without crack growth. The compliance, λ_0, was determined by substituting a_0 and λ into Eq.(2), where a_0 is initial notch depth. Next, the compliance, λ, during crack growth was calculated from each data point of the applied load vs. back-face strain curve. Substituting λ into Eq.(2) again, the change of crack length, a, for the applied load, P, was obtained. Subsequently, the stress intensity factor, K_R, for the crack length, a, was calculated by the following equation[9], and then R-curve behavior was derived from the relationship between the calculated K_R and the amount of crack extension, Δa $(=a-a_0)$:

$$K_R=\frac{3P(S_1-S_2)}{2BW^2}F(\alpha)\sqrt{\pi a} \qquad (4)$$

where $F(\alpha)$ is dimensionless geometric factor. $F(\alpha)$ is given by

$$F(\alpha)=\sqrt{\frac{2}{\pi\alpha}\tan\left(\frac{\pi\alpha}{2}\right)}\frac{0.923+0.199\left(1-\sin\frac{\pi\alpha}{2}\right)^4}{\cos\frac{\pi\alpha}{2}}. \qquad (5)$$

In the present study, only one crack was assumed to propagate straightly from the notch tip, even though the crack did not always propagate straightly. The compliance change was assumed to be entirely caused by the stable crack growth[3].

References

(1) Introduction Lectures IX 'Coal Utilization Combined Cycle IGCC/PFBC', Thermal and Nuclear Power, (in Japanese), Vol. 49, No. 1 (1998), pp. 103-127.

(2) Ishioka, H., Ohnishi, T., Akiyama, H., Kato, M. and Makiura, S., Thermal and Nuclear Power, (in Japanese), Vol. 50, No. 3 (1999), pp. 318-324.

(3) Tanaka, K., Akiniwa, Y., Nomura, T. and Sakaida, Y., Trans. Jpn. Soc. Mech. Eng., (in Japanese), Vol. 65, No. 640, A (1999), pp. 2385-2392.

(4) Sakaida, Y. and Tanaka, K., J. Soc. Mater. Sci. Jpn., (in Japanese), Vol. 49, No. 3 (2000), pp. 304-309.

(5) Awaji, H. and Sakaida, Y., J. Am. Ceram. Soc., Vol. 73, No. 11 (1990), pp. 3522-3523.

(6) Song, D. and Takeda, N., Progress Reports of Fiscal 1997 for "Research on Improvement of Reliability of High-Temperature Material for High-Efficient Power Generator", (1998), pp. 51-62, JFCC.

(7) Kunio, T., Nakazawa, H., Hayashi, I. and Okamura, H., Fracture Mechanics Experimental Techniques, (1990), p. 128, Asakura-syoten.

(8) Hiramatsu, K., Okada, A. and Usami, H., Proc. 22nd Annual Conf. on Composites, Advanced Ceramics, Materials, and Structures, B (ed. by D. Bray), J. Am. Ceram. Soc., Cocoa Beach, (1998), pp. 335-340.

(9) Tada, H., Paris, P.C. and Irwin, G., The Stress Analysis of Crack Handbook, (1985), pp. 2-14, Del Res. Corp.